iScience

CellPress
OPEN ACCESS

Article

DLX2 promotes osteosarcoma epithelial-mesenchymal transition and doxorubicin resistance by enhancing HOXC8-CDH2 axis

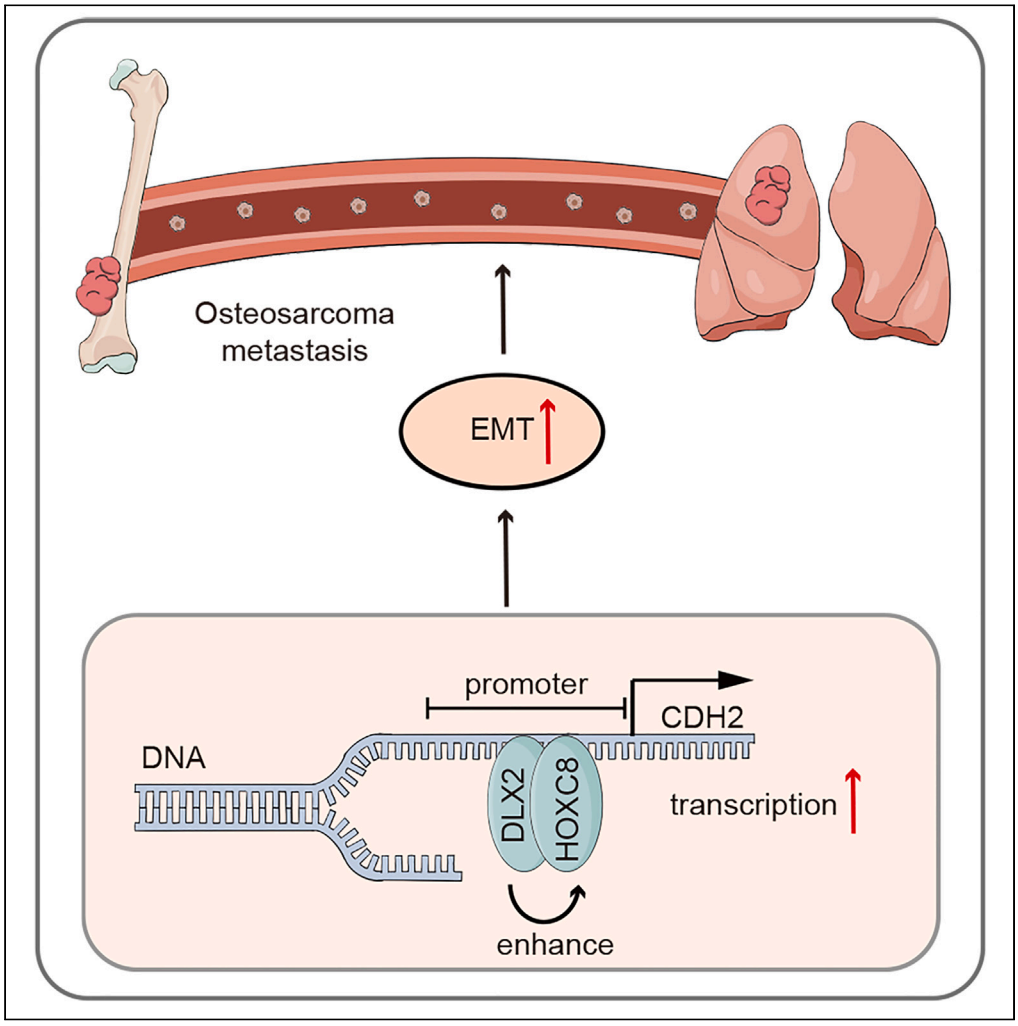

Boya Zhang, Xinhui Du, Yichao Fan, Guoxin Qu, Lon Kai Pang, Ruiying Zhao, Weitao Yao

zlyyzhangboya@163.com (B.Z.)
zlyyyaoweitao1402@zzu.edu.cn (W.Y.)

Highlights

DLX2 is significantly upregulated in metastatic osteosarcoma

DLX2 enhances CDH2 transcription

DLX2 enhances doxorubicin resistance

Zhang et al., iScience 26, 108272
November 17, 2023
https://doi.org/10.1016/j.isci.2023.108272

iScience

CellPress
OPEN ACCESS

Article

DLX2 promotes osteosarcoma epithelial-mesenchymal transition and doxorubicin resistance by enhancing HOXC8-CDH2 axis

Boya Zhang,[1,4,5,*] Xinhui Du,[1,4] Yichao Fan,[1] Guoxin Qu,[1] Lon Kai Pang,[2] Ruiying Zhao,[3] and Weitao Yao[1,*]

SUMMARY

Metastasis and doxorubicin resistance are challenges in the clinical diagnosis and treatment of osteosarcoma, the mechanisms underlying these phenomena remain unclear. In this study, we found that DLX2 is highly expressed in metastatic osteosarcoma and is closely related to clinical prognosis. Knockdown of DLX2 inhibited tumor proliferation and migration *in vitro* and inhibited tumor growth *in vivo*. Mechanistically, we found that DLX2 enhanced the repression of CDH2 transcription by binding to HOXC8, thereby promoting the epithelial-mesenchymal transition in osteosarcoma cells. Through subsequent exploration, we found that targeting DLX2/HOXC8 signaling significantly restores the sensitivity of osteosarcoma cells to doxorubicin. In conclusion, our findings demonstrate that DLX2 may enhance the transcriptional regulation of CDH2 through interacting with HOXC8, which in turn promotes epithelial-mesenchymal transition and doxorubicin resistance in osteosarcoma. These findings hold great potential for clinical application and may guide the development of novel targeted therapies for osteosarcoma.

INTRODUCTION

Osteosarcoma (OS) stands as the most prevalent primary malignant bone tumor in adolescents. Despite its increasing incidence, treatment strategies have seen limited evolution.[1] Currently, the principal clinical approaches for OS encompass surgical resection and comprehensive chemotherapy. The metastasis of OS, following an incomplete response to chemotherapy, remains a significant challenge due to its propensity to spread to adjacent tissues and distant sites, including the lungs. Although the five-year survival rate for OS has improved to approximately 70% since the introduction of the chemotherapeutic trio consisting of methotrexate, doxorubicin, and cisplatin (MAP), newly diagnosed patients with metastatic disease, relapsed cases, or individuals unresponsive to MAP therapy exhibit a five-year survival rate of only around 20%.[2,3] Consequently, much remains to be comprehended regarding the fundamental mechanisms governing the development and progression of OS. The elucidation of these frameworks is imperative for the advancement of novel treatments that can significantly enhance patient outcomes.

The epithelial-mesenchymal transition (EMT) stands as a pivotal hallmark of tumor progression, entailing a multitude of tumor-related functions, including tumor initiation, malignant advancement, tumor stemness, metastasis, and therapy resistance.[4–6] To gauge the EMT status in tumor cells, E-cadherin (CDH1), N-cadherin (CDH2), and vimentin (VIM) are commonly employed. Elevated CDH1 expression typically signifies EMT inhibition, while heightened CDH2 and vimentin expression serve as prominent EMT indicators. Notably, EMT plays a crucial role in osteosarcoma (OS), where several key genes, such as TWIST, SNAIL, and those within the ZEB family, have been identified as regulators of OS metastasis through EMT.[7–9] Additionally, a study by Wang T et al. has demonstrated that the TGFβ-miR-499a-SHKBP1 signaling pathway can induce OS resistance to EGFR inhibitors by fostering EMT.[10] Nonetheless, the mechanisms and regulatory pathways governing EMT in OS remain poorly comprehended. Consequently, EMT in OS represents an unexplored reservoir of potential therapeutic targets, the elucidation of which has the potential to catalyze significant breakthroughs in OS treatment.

In this study, our investigation unveiled a novel role of DLX2 in promoting EMT in OS through its interaction with HOXC8, subsequently leading to an enhancement in CDH2 transcription. Notably, our study identified a substantial overexpression of DLX2 in metastatic OS, demonstrating a close correlation with cross-clinical prognostic data. Through a series of phenotypic assays, we validated that the knockdown of DLX2 yielded a significant inhibition of OS cell proliferation and migration *in vitro*, along with a noticeable reduction in tumor growth *in vivo*. Combining predictive computational models with *in vitro* experiments, we elucidated the formation of a DLX2-HOXC8 complex, which synergistically amplifies CDH2 transcription, thereby fostering the EMT process in OS. Furthermore, our investigation also unveiled that targeting

[1]Department of Bone and Soft Tissue Oncology, The Affiliated Cancer Hospital of Zhengzhou University & Henan Cancer Hospital, Zhengzhou 450008, China
[2]Baylor College of Medicine, Houston, TX 77030, USA
[3]Department of Intergrative Biology & Pharmacology, McGovern Medical School, The University of Texas Health Science Center at Houston, Houston, TX 77030, USA
[4]These authors contributed equally
[5]Lead contact
*Correspondence: zlyyzhangboya@163.com (B.Z.), zlyyyaoweitao1402@zzu.edu.cn (W.Y.)
https://doi.org/10.1016/j.isci.2023.108272

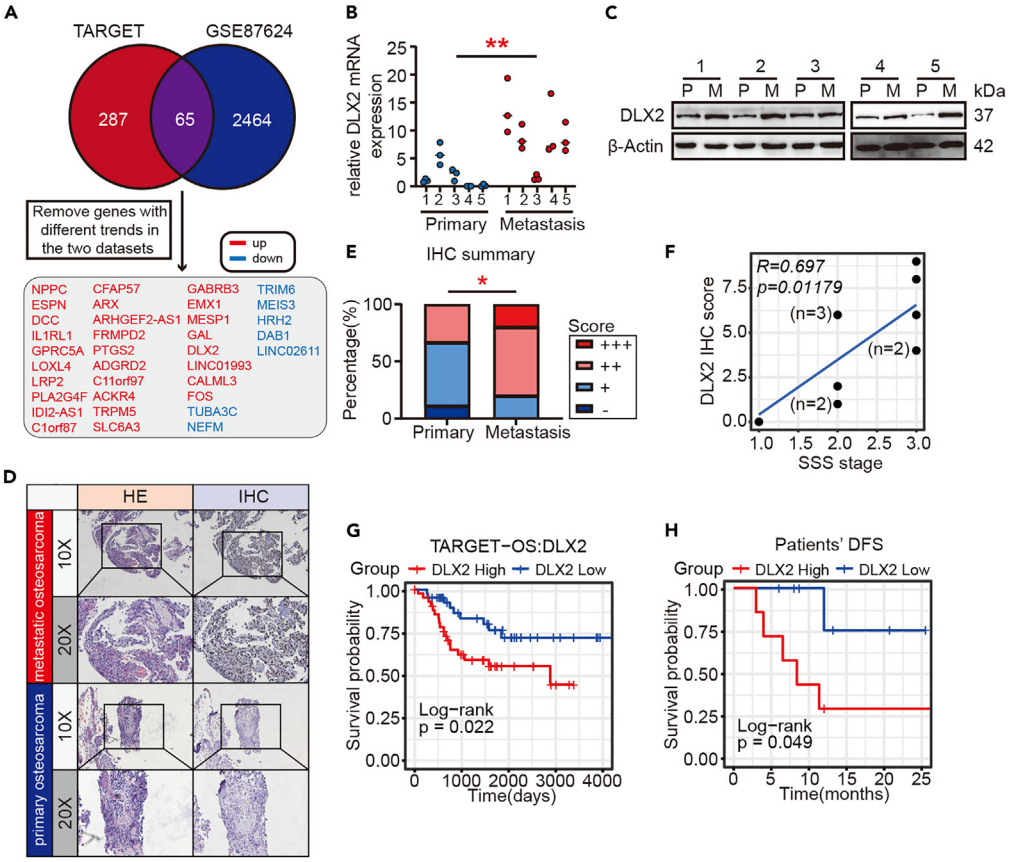

Figure 1. Clinical significance of DLX2

(A) Upper Venn plot shows the intersect result of DEGs in TARGET and GSE87624 dataset. Lower panel shows the intersect genes after removing genes with different trends in two dataset, genes in red refers to significantly upregulated, whereas blue refers to significantly downregulated.

(B) qPCR results of DLX2 expression in primary and metastatic osteosarcoma tissue.

(C) Western blot of the DLX2 protein expression in primary and metastatic osteosarcoma tissue. "P" is for primary osteosarcoma, "M" is for metastatic osteosarcoma.

(D) Immunohistochemistry of DLX2 expression in patient tissues, HE were done in continuous slices.

(E) The summary of IHC scores, presented in percentage. "-": negative; "+": weak positive; "++": positive; "+++": strong positive.

(F) Relationship between DLX2 IHC score and SSS stage.

(G) Overall survival of patients in TARGET database with high or low DLX2 expression.

(H) Disease-free survival (DFS) of patients we collected with high or low DLX2 expression. Error bars shown in the figure represent the mean ± SEM.

DLX2 substantially heightens the sensitivity of drug-resistant tumor cells to doxorubicin, both *in vitro* and *in vivo*. By shedding light on this previously undiscovered mechanism of EMT regulation in OS, our study lays the foundation for identifying innovative therapeutic targets for the treatment of metastatic OS.

RESULTS

DLX2 is upregulated in metastatic osteosarcoma and is associated with poor clinical outcomes

To comprehensively screen for gene expression patterns specific to OS metastasis, we analyzed differentially expressed genes (DEGs) between metastatic and localized OS using the TARGET and GSE87624 datasets. A total of 35 DEGs were identified across both datasets, including 28 significantly upregulated and 7 significantly downregulated genes in metastatic compared to localized OS (threshold: |logFC| >1, p value < 0.05, Figure 1A). Among these genes, DLX2 was of particular interest. DLX2 belongs to the NK-like family and exerts dual roles in development and cancer; however, its role in OS is still unknown. Therefore, our team decided to further investigate DLX2.

To validate the results of our initial analysis, we collected samples from 12 patients with OS (5 metastasized, 7 localized, Table 1) and examined the expression of DLX2. We found that, compared to localized OS, DLX2 transcripts and protein products were significantly higher in metastatic OS (Figures 1B and 1C), and immunohistochemical results suggested a higher proportion of metastatic OS cells overexpressed DLX2 overexpression (Figures 1D and 1E). In addition, we found that DLX2 expression was also significantly increased in patients with higher surgical staging system (SSS) stage, suggesting that DLX2 may potentially be associated with OS progression (Figure 1F). We then performed

Table 1. DLX2 expression level and main characteristics of the OS patients (n = 12)

Characteristic	n(n%)	DLX2 IHC score (mean)	p-value[a]
Gender			
Male	7 (58.33%)	4.71	0.9490
Female	5 (41.67%)	4.6	
Age			
0–10	2 (16.67%)	4	0.7344
11–20	10 (83.33%)	4.8	
SSS stage			
1	1 (8.33%)	0	**0.048**
2	6 (50.00%)	3.67	
3	5 (41.67%)	6.6	
Metastasis			
Yes	5 (64.29%)	6.6	**0.0387**
No	7 (35.71%)	3.28	
Disease-free survival status			
Disease-free	6 (50.00%)	2.83	**0.0161**
Progress	6 (50.00%)	6.5	

[a]Significance threshold: p-value<0.05. All p-values with significant differences are bolded.

Kaplan-Meier survival analysis using the TARGET database and clinical data obtained from patients. We found that patients with increased expression of DLX2 had significantly worse survival (Figure 1G and 1H). Taken together, these results show that DLX2 was significantly overexpressed in metastatic OS and was closely associated with poor clinical prognosis, suggesting that DLX2 may play an important role in OS progression to metastasis.

DLX2 depletion inhibits tumor proliferation and migration *in vitro* and tumor growth *in vivo*

Next, we examined the expression of DLX2 in OS cell lines. We found that compared to normal human osteoblast cells hFOB-1.19, DLX2 was significantly upregulated in the osteosarcoma cell lines U2-OS, MG63, and 143B (Figure 2A). Subsequent experiments were conducted using U2-OS and 143B cells. First, we knocked down DLX2 in these two cell lines using lentiviral vectors (Figures 2B and 2C) and assessed the biological functions of the cells using CCK-8 assays (Figures 2D and 2E), colony formation assays (Figures 2F–2I), and Transwell assays (Figures 2J–2 M). The results showed that knocking down DLX2 significantly inhibited the proliferation and migration abilities of U2-OS and 143B cells. Subsequent detection of PCNA and caspase-3 levels indicated limited impact on apoptosis in these cell lines (Figure S1A).

To further investigate the *in vivo* effects of DLX2 on tumor proliferation and migration, we conducted two animal experiments. Firstly, we established cell-derived xenografts by subcutaneously injecting tumor cells into nude mice. After successful tumor formation, we intratumorally injected adenoviruses (AAV) to knock down DLX2, and we observed a significant inhibition of tumor growth after DLX2 knockdown (Figures 2N–2P). Secondly, we established an osteosarcoma lung metastasis model by injecting tumor cells into the tail veins of mice. We found that knocking down DLX2 significantly reduced the size of lung metastases (Figures 2Q–2R). These results suggest that knocking down DLX2 can inhibit tumor cell proliferation and migration *in vitro* and suppress tumor growth and lung metastasis *in vivo*.

DLX2 promotes tumor epithelial-mesenchymal transition by enhancing HOXC8-mediated CDH2 transcription

We then sought to explore the mechanisms by which DLX2 impairs the migration ability of OS cells. The epithelial-mesenchymal transition (EMT) is an important step in tumor metastasis, and genes including CDH1, CDH2, and vimentin have been implicated. Following DLX2 depletion, we found that the RNA expression of CDH1 was increased in the U2-OS cell line but not in the 143B cell line; CDH2 RNA was significantly downregulated in both cell lines; and vimentin did not show any significant change at the RNA level (Figures 3A and 3B). At the protein level, with the knockdown of DLX2, the expression of CDH1 showed no change, while on the contrary, the protein expressions of CDH2 and vimentin were significantly downregulated. These results suggest that DLX2 depletion can significantly affect the expression of key genes involved in EMT (Figure 3C). Subsequently, we utilized Genemania and Hitpredict databases to generate predictions of proteins that bound DLX2. Intersecting the database results revealed four proteins with the potential to bind DLX2: MSX1, MSX2, HOXC8, and DLX5 (Figure 3E). Since MSX1, MSX2, and DLX5 have previously been reported to interact with DLX2, we focused our investigative efforts on HOXC8.

We next analyzed the effect of HOXC8 depletion on EMT-related genes using GSE133780. The results suggested that CDH2 and TWIST1 were significantly decreased following knockdown of HOXC8, while MMP2 was significantly upregulated (Figure 3D). Subsequently, we knocked down DLX2 or HOXC8 in U2-OS and 143B cell lines, respectively, and found that while CDH2 RNA and protein levels were

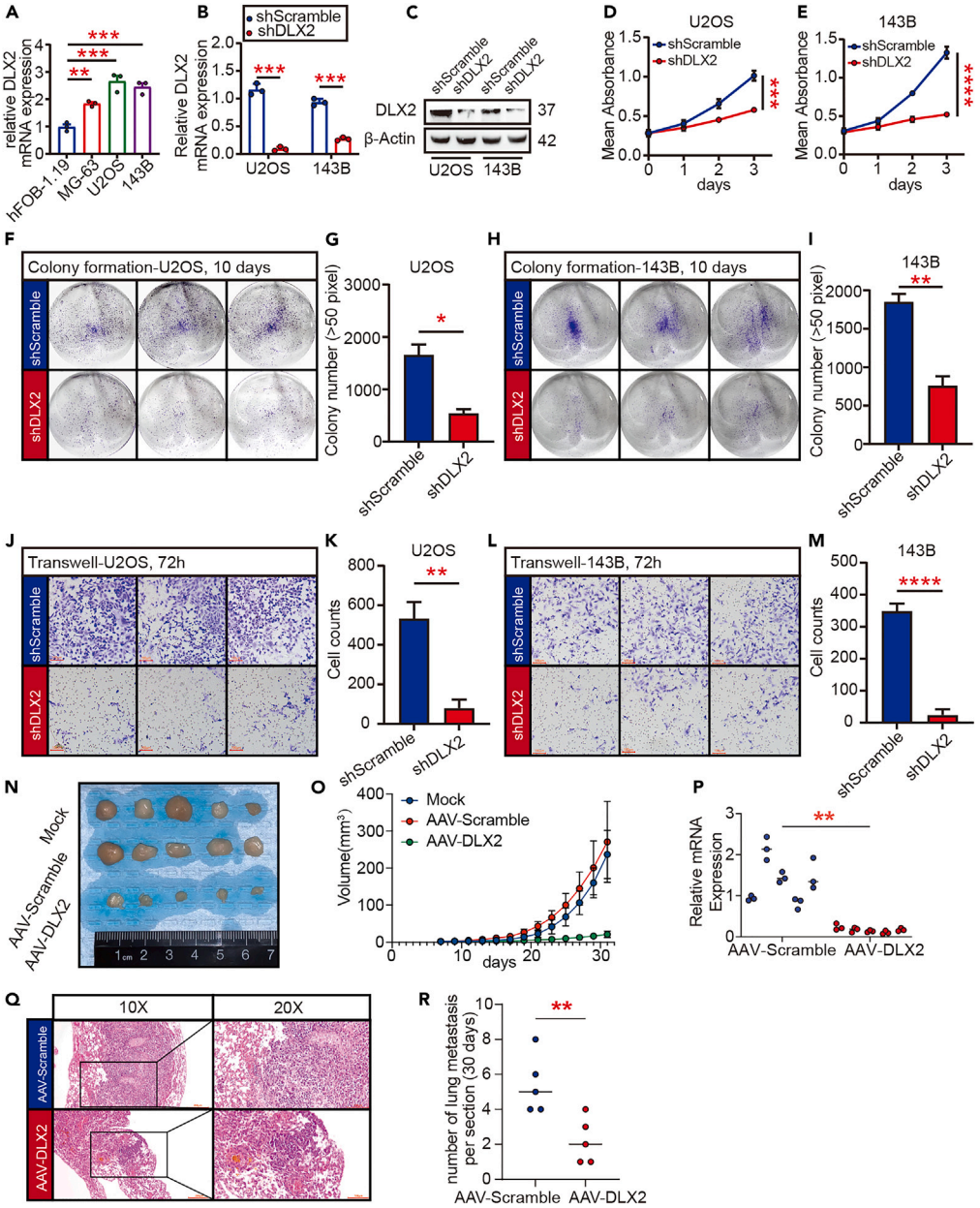

Figure 2. Phenotypes of DLX2 depletion *in vitro* and *in vivo*

(A) DLX2 mRNA expression in hFOB-1.19, U2OS,MG-63, and 143B cell lines.

(B) DLX2 depletion efficiency detection using qPCR.

(C) DLX2 depletion efficiency detection using western blot.

(D and E) Cell viability before/after DLX2 depletion using CCK-8.

(F–I) colony formation assay shows the proliferation ability of OS cells before/after DLX2 depletion.

(J–M) Transwell assay shows the migration ability of OS cells before/after DLX2 depletion.

(N) transplant tumors after *in vivo* experiment. Mock refers to cells without any treat, AAV-Scramble refers to cells treated with AAV containing scramble sequence, AAV-DLX2 refers to cells containing sequence targeting DLX2.

(O) tumor volume of corresponding groups.

(P) DLX2 mRNA expression in transplant tumors of each group.

(Q) After tail vein injection of the corresponding cells, HE staining results showing the lung tumor formation. Pictures were taken under a 10X and 20X objective, respectively.

(R) Statistical graph of lung tumor count observed based on HE staining at 30 days. Error bars shown in the figure represent the mean ± SEM.

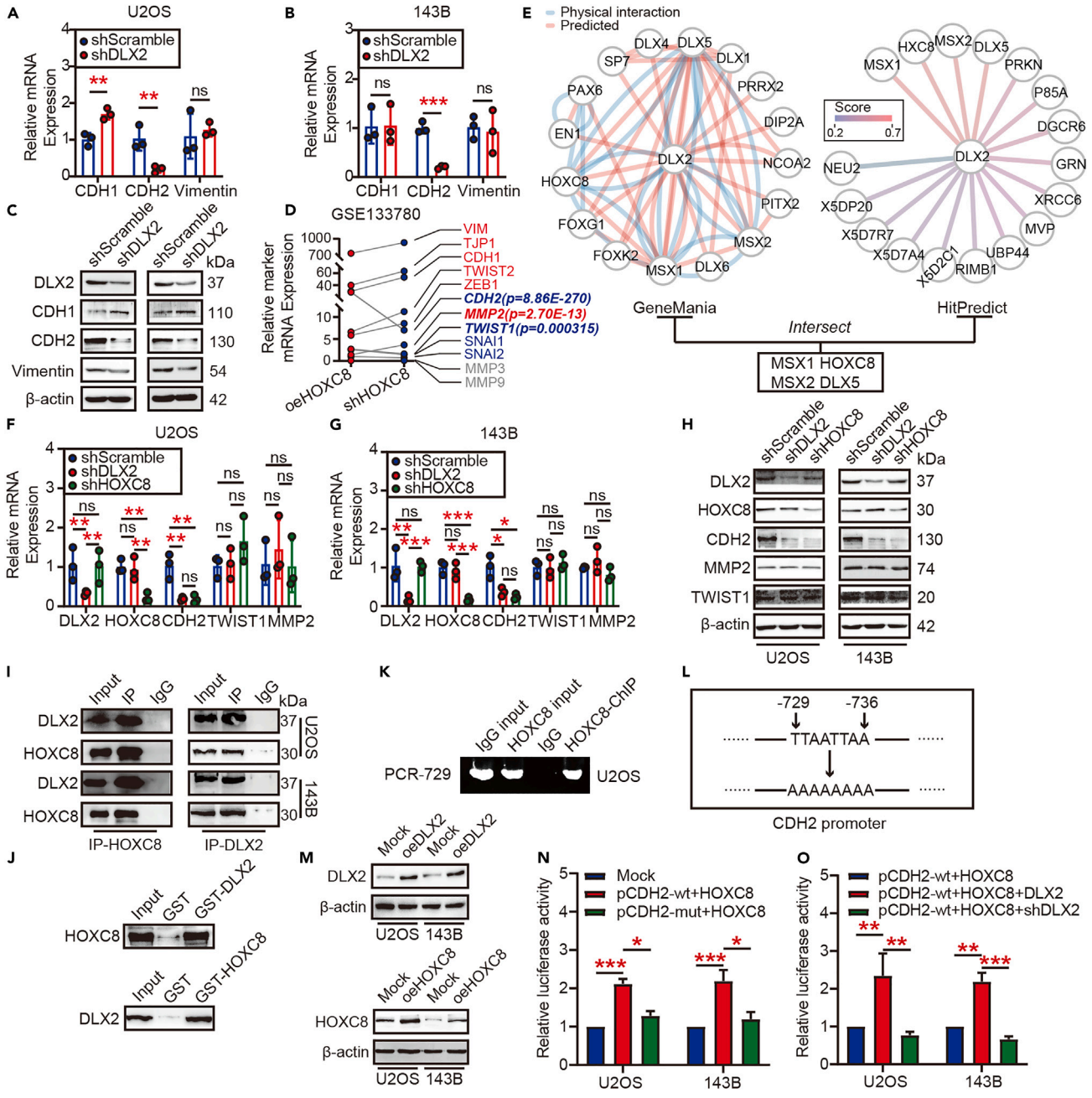

Figure 3. DLX2 promotes osteosarcoma EMT by enhancing CDH2 transcription through binding with HOXC8

(A and B) corresponding EMT-related mRNA expression after DLX2 knock down.

(C) corresponding EMT-related protein expression after DLX2 knock down.

(D) EMT-related gene expression between HOXC8 depletion and overexpression groups in GSE133780 dataset. Genes in red refers to upregulated, genes in blue refers to downregulated, genes marked in bold refers to be significant (p value <0.05).

(E) Intersect result of DLX2-binding proteins predicted by GeneMania and HitPredict websites.

(F and G) mRNA expression of corresponding genes before/after DLX2 or HOXC8 depletion.

(H) Protein expression of corresponding genes before/after DLX2 or HOXC8 depletion.

(I) Immunoprecipitation results confirm the interaction between HOXC8 and DLX2.

(J) GST pull-down results indicate the interaction between HOXC8 and DLX2.

(K) Agarose gel results of ChIP-PCR using HOXC8 antibody and corresponding primers.

(L) Binding site mutation.

(M) DLX2 and HOXC8 overexpression efficiency.

Figure 3. *Continued*

(N) Dual luciferase assay. Mock: no treatment; pCDH2-wt+HOXC8: wild-type CDH2 promoter and HOXC8 overexpression; pCDH2-mut+HOXC8: mutation CDH2 promoter (729–736) and HOXC8 overexpression.

(O) Dual luciferase assay was done to validate the mechanism of DLX2 in HOXC8 mediated CDH2 transcription. Error bars shown in the figure represent the mean ± SEM.

significantly reduced, no significant changes were observed in TWIST1 and MMP2. This suggests that DLX2 and HOXC8 may regulate OS EMT through CDH2 regulation (Figures 3F–3H). The results of nuclear-cytoplasmic fractionation indicate that DLX2 is primarily expressed in the cell nucleus, while HOXC8 shows higher expression in the cell nucleus (Figure S1B). This provides evidence for a potential relationship between the two. In addition, we verified the predictive model by confirming through co-immunoprecipitation and GST pulldown that HOXC8 binds directly to DLX2. These findings collectively suggest that DLX2 may form a complex with HOXC8 to enhance the transcription of CDH2 (Figures 3I and 3J).

To further explore this mechanism, we generated predictions for the binding site of HOXC8 to the CDH2 promoter region (within 1.5 kb upstream of the transcription start site) through the JASPAR database. We screened sites with a binding probability of more than 90% (Table 2). We designed corresponding PCR primers for the top ranked potential site at 729–736, marked as "PCR-729". Subsequently, we enriched HOXC8-bound DNA through ChIP and quantified them with PCR. The results showed that the sequence corresponding to PCR-729 was bound to HOXC8 (Figure 3K). To further verify this conclusion, we modified the sequence of this potential binding site and performed a dual-luciferase reporter assay (Figure 3L). Firstly, we found that DLX2-and HOXC8-expressing plasmids can significantly increase the expression of those genes in tumor cells (Figure 3M). Secondly, the dual-luciferase reporter assay showed that the transcriptional capacity of the wild-type sequence (pCDH2-wt) was significantly enhanced after overexpression of HOXC8, while the luciferase decreased significantly upon modifying this site (pCDH2-mut) (Figure 3N).

We also found that the transcriptional capacity of pCDH2-wt was significantly reduced when DLX2 overexpression was replaced with shRNA-mediated DLX2 depletion, suggesting that DLX2 expression is critical for HOXC8-mediated CDH2 transcription. However, this reduced level (pCDH2-wt+HOXC8+shDLX2) was not significantly lower than the blank control (pCDH2-wt+HOXC8), suggesting that there may be other factors that affect HOXC8 (Figure 3O). Regardless, our results show that DLX2 enhances HOXC8-mediated CDH2 transcription by binding to HOXC8, and HOXC8 regulates CDH2 by binding to the 729–736 site in the CDH2 promoter region.

HOXC8 depletion represses osteosarcoma metastasis and EMT

Based on the aforementioned results, we hypothesized that HOXC8 may play a role in the biological functions of OS cells as well as their EMT. We overexpressed and knocked down HOXC8 respectively *in vitro* (Figures 4A and 4B), and confirmed by CCK8 (Figures 4C and 4D), colony formation (Figures 4E and 4F) and Transwell (Figures 4G and 4H) experiments that compared with overexpression of HOXC8, HOXC8 depletion significantly inhibited the proliferation and migration of U2-OS and 143B cells. Further experiments showed that after knocking down HOXC8, the expression levels of CDH2 and vimentin were significantly decreased (Figures 4I–4K). Interestingly, the results in Figures 4I and 4J are different from those in Figures 3A and 3B, suggesting that HOXC8 may regulate vimentin transcription through other means. The DLX2-HOXC8 complex may only regulate the transcription of CDH2. Taken together, our results demonstrate that HOXC8 significantly affects the biological functions and EMT of OS cells.

Targeting DLX2 enhances doxorubicin response in OS

Previous studies have shown a strong link between EMT and doxorubicin sensitivity, particularly that EMT often leads to the development of doxorubicin resistance. Our findings thus far prompted us to explore the potential association between DLX2-HOXC8 complex-mediated EMT in OS and doxorubicin sensitivity.

Table 2. HOXC8-CDH2 prediction binding results of JASPAR database

Score	Relative score	Start	End	Strand	Predicted sequence
9.720072	0.970341	729	736	+	TTAATTAA
9.720072	0.970341	729	736	–	TTAATTAA
9.720072	0.970341	816	823	+	TTAATTAA
9.720072	0.970341	816	823	–	TTAATTAA
7.964231	0.935431	4	11	+	TTCATTAA
7.964231	0.935431	1036	1043	+	TTCATTAA
7.926544	0.934682	4	11	–	TTAATGAA
7.926544	0.934682	1036	1043	–	TTAATGAA
7.638196	0.928949	1046	1053	+	GCAATGAA
7.627415	0.928735	1046	1053	–	TTCATTGC

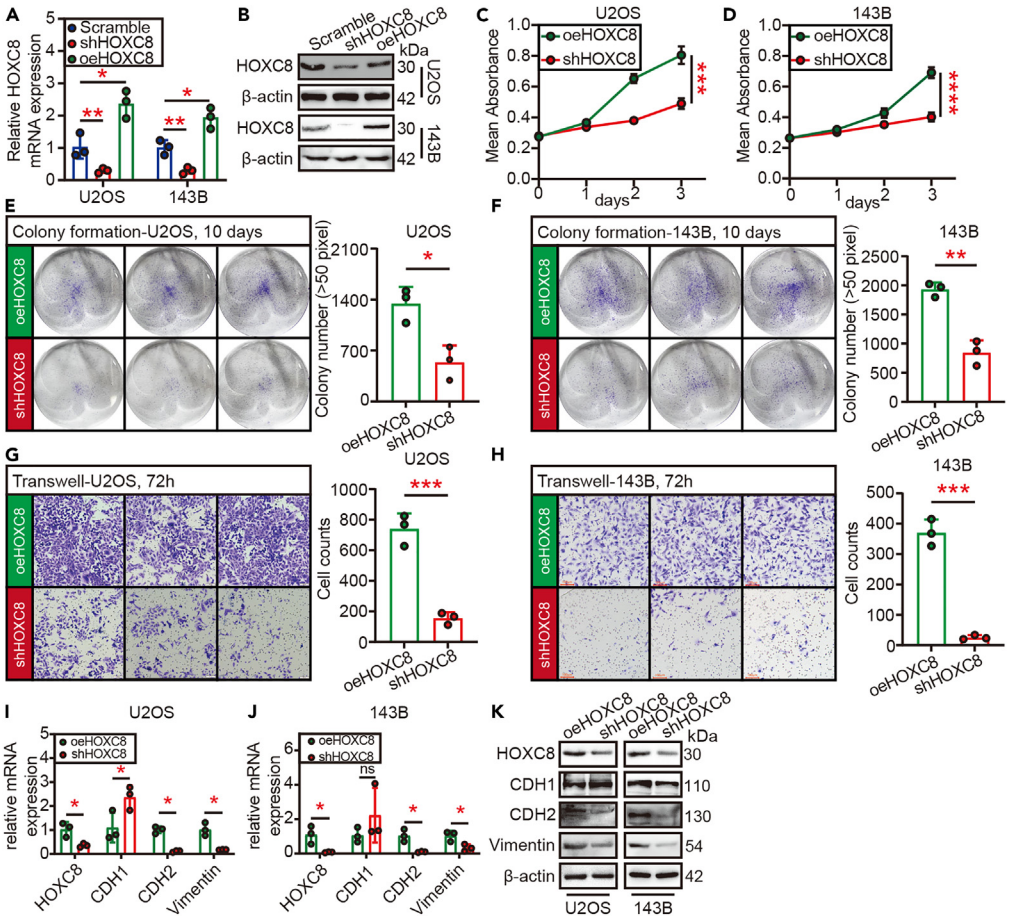

Figure 4. HOXC8 depletion inhibits osteosarcoma EMT

(A) HOXC8 mRNA depletion and overexpression efficiency.

(B) HOXC8 protein depletion and overexpression efficiency.

(C and D) cell viability changes between HOXC8 overexpression and HOXC8 depletion were detected by CCK-8.

(E and F) colony formation assay was used to test proliferation ability of HOXC8 overexpression cells and HOXC8 depletion cells.

(G and H) Transwell assay was used to test proliferation ability of HOXC8 overexpression cells and HOXC8 depletion cells.

(I and J) EMT-related genes' mRNA expression in HOXC8 overexpression and depletion OS cells.

(K) EMT-related genes' protein expression in HOXC8 overexpression and depletion OS cells. Error bars shown in the figure represent the mean ± SEM.

We first treated DLX2-knockdown and negative control U2-OS and 143B cells with 0–6.4 ug/mL or 0 - 9.6 ug/mL doxorubicin for 24 h, respectively, and assessed cell viability at different concentrations of doxorubicin with CCK8 (Figures 5A and 5B). We found that DLX2 depletion can significantly reduce the survival rate of U2-OS and 143B cells treated with doxorubicin. This suggested a relationship between DLX2 expression and the sensitivity of OS cells to doxorubicin. To explore the clinical potential of this finding, we constructed a doxorubicin-resistant U2-OS cell line (U2OS-DoxR, details in methods). We found that the expressions of DLX2 and CDH2 were upregulated in U2OS-DoxR compared with U2OS, but the expression of HOXC8 was not significantly increased. Furthermore, knockdown of DLX2 in U2OS-DoxR (DoxR-shDLX2) significantly reduced CDH2 protein and mRNA expression, which was consistent with our previous results (Figures 5C and 5D).

To further explore the effect of DLX2 on doxorubicin resistance, we divided the cells into three groups: (1) U2OS; (2) U2OS-DoxR; (3) DoxR-shDLX2. Each group of cells was treated with 0.5 ug/mL doxorubicin or DMSO, and cell viability was verified with CCK8 assay. The results showed that U2OS and DoxR-DLX2 did not survive following doxorubicin treatment when compared to DMSO treatment ($p < 0.0001$, $p < 0.0001$, respectively), whereas U2OS-DoxR continued to grow ($p = 0.1269$). Furthermore, upon addition of doxorubicin, DoxR-shDLX2 cell proliferation was significantly decreased compared to U2OS-DoxR, though the DoxR-shDLX2 population continued to grow slowly. Still, our results suggest that knockdown of DLX2 can significantly increase doxorubicin sensitivity in OS (Figure 5E).

We further explored the aforementioned conclusions *in vivo*. After establishing cell-derived xenografts using U2OS-DoxR cells, we intravenously injected doxorubicin and found that knocking down DLX2 significantly reduced tumor volume. This indicates that targeting DLX2 can partially restore the sensitivity of drug-resistant cells to doxorubicin (Figures 5F and 5H). Subsequently, we performed immunohistochemistry to assess the expression of DLX2 and CDH2. The results showed that knocking down DLX2 significantly reduced the expression of CDH2

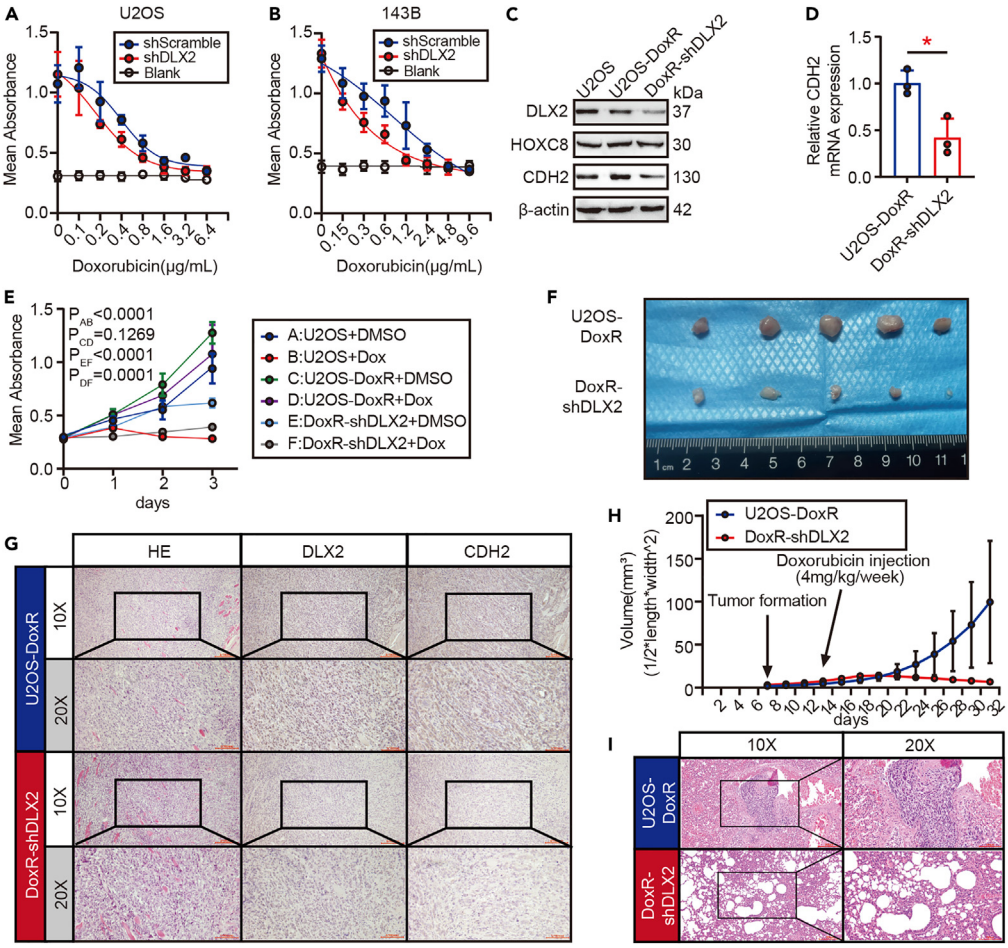

Figure 5. DLX2 restore OS doxorubicin sensitivity by inhibiting EMT

(A and B) Drug toxicity test of U2OS and 143B with doxorubicin.

(C) Protein expression of indicated genes in U2OS, doxorubicin resistant U2OS (U2OS-DoxR) and U2OS-DoxR with DLX2 depletion (DoxR-shDLX2).

(D) CDH2 mRNA expression in U2OS-DoxR and DoxR-shDLX2.

(E) CCK-8 assay of indicated groups.

(F) Subcutaneous xenografts of the doxorubicin-resistant cell line (DoxR-Scramble) and the doxorubicin-resistant cell line with DLX2 knockdown (DoxR-shDLX2) after one month of doxorubicin treatment, with a ruler shown below for scale.

(G) HE staining of the tumor and immunohistochemical staining for DLX2 and CDH2 at corresponding locations, using consecutive sections.

(H) Tumor growth curves for the respective groups. Doxorubicin injections began on the 13th day at a dose of 4 mg/kg per week.

(I) Establishment of lung metastasis models by intravenous injection of doxorubicin-resistant OS cells using the doxorubicin-resistant cell line (DoxR-Scramble) and the DLX2 knockdown doxorubicin-resistant cell line (DoxR-shDLX2), followed by the administration of doxorubicin for one month at a dose of 4 mg/kg per week. Lung tissues were then extracted for HE staining. Error bars shown in the figure represent the mean ± SEM.

(Figure 5G). This effect was even more significant in the lung metastasis model. After knocking down DLX2, we did not observe tumor formation in the lung tissues of the mice in the knockdown group throughout the experiment. In contrast, the U2OS-DoxR cells in the control group formed lung metastases without any issues (Figure 5I). This suggests that knocking down DLX2 may have a significant inhibitory effect on the lung metastasis of drug-resistant cells.

In all, our study demonstrated that DLX2 may promote CDH2 transcriptional upregulation by forming a complex with HOXC8, thereby inducing EMT and promoting doxorubicin resistance in OS. Targeting DLX2 may serve as a new potential therapeutic target and provide new ideas for the treatment of doxorubicin-resistant OS patients.

DISCUSSION

In this study, we demonstrated through *in vitro* and *in vivo* experiments that DLX2 promotes OS EMT and doxorubicin resistance. Mechanistically, DLX2 promotes the transcription of CDH2 by binding to HOXC8, and HOXC8 binds within the 729–736 nucleotide sequence of the

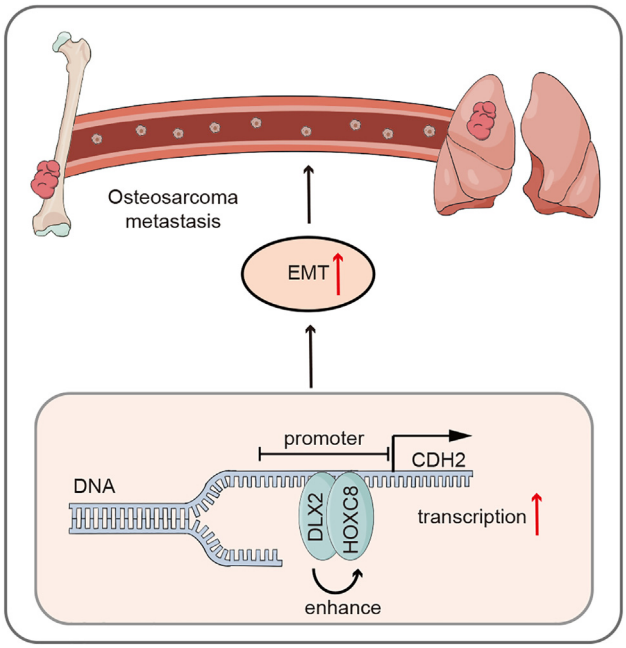

Figure 6. The schematic diagram represents the mechanism of this study

DLX2 enhances the transcription of CDH2 by binding to HOXC8, thereby promoting osteosarcoma metastasis and doxorubicin resistance.

CDH2 promoter region. Our study helps to reveal the underlying mechanism of OS metastasis and provides a new potential target for the treatment of OS (Figure 6).

Metastasis of OS remains a significant issue in clinical management of patients with OS. Metastasis is mediated by abnormal gene and protein expression, which fundamentally alters the function of OS cells.[11–16] In the past few decades, several studies have revealed the underlying mechanism of OS metastasis, resulting in the development of therapeutic drugs. For example, tyrosine kinase inhibitors (TKIs) including apatinib, axitinib, and cabozantinib inhibit OS metastasis by targeting molecules such as VEGFR, PDGFR, and RET.[17] Recently, Wang X et al. found that pyrvinium pamoate, a selective activator of CK1α, can inhibit OS metastasis through the CK1α/CBX4 axis and that targeting the CK1α/CBX4 axis may benefit patients with OS metastasis.[18] Motonari N et al. confirmed that Tegavivint, a novel β-catenin/TBL1 inhibitor, can effectively treat metastatic OS by targeting the β-catenin/ALDH1 axis.[19] Despite these advancements, much about OS metastasis remains unclear, warranting continued investigation. In this study, we confirmed through a series of *in vitro* and *in vivo* experiments, utilizing OS cell lines and patient tumor tissues that DLX2 was significantly highly expressed in metastatic OS and was closely associated with poor prognosis. Targeting DLX2 can significantly inhibit the migration ability of tumor cells. This suggests that DLX2 may play an important role in OS metastasis, and these results lay the foundation for our further exploration of the mechanism.

The DLX homeobox family of genes encodes transcription factors that play an integral role in embryonic and postnatal development.[20–23] DLX genes are also involved in the coordination of hematopoiesis and,[24] when dysregulated, may be involved in the regulation of tumorigenesis and progression. Aberrant expression of the DLX gene is associated with hematological malignancies, including leukemia and lymphoma. In T cell lymphomas, Dlx5 has been shown to act as an oncogene by cooperating with activated Akt, Notch1/3, and/or Wnt to drive tumorigenesis[24,25]. DLX2 has also been confirmed to be involved in the regulation of multiple important pathways. Increased expression of DLX2 induced the upregulation of SNAIL, whereas knockdown of DLX2 blocked TGFβ-induced epithelial-mesenchymal transition.[26] In glioblastoma multiforme (GBM) patients, high levels of DLX2 are associated with poorer survival, and knockdown of DLX2 in GBM cells reduces cyclin D1 expression.[27] However, the role of DLX2 in OS had yet to be explored. In this study, we combined bioinformatics prediction and *in vitro* experiments to confirm that DLX2 promotes the EMT process of OS and doxorubicin resistance by binding and enhancing the transcription of HOXC8 to CDH2, and we further confirmed by ChIP-PCR and dual-luciferase reporter assay that HOXC8 binds at bases 729–736 of the CDH2 promoter region. Our study elucidates the interactions between molecules and helps to gain insight into the underlying mechanisms of OS metastasis.

Cancer-related EMT has been confirmed to be deeply involved in the progression of carcinoma and sarcoma, especially in metastasis.[28,29] TWIST has been reported to regulate EMT and cisplatin resistance in OS cells by participating in β-catenin signaling and endothelin-1/endothelin A receptor signaling.[7,30] Another study indicated that TWIST1 can promote the invasion of OS cells by inhibiting the expression of TIMP1.[31] In addition, other important factors in the EMT process, such as SNAIL and Zeb family, have also been reported to be involved in the regulation of OS metastasis.[8,32,33] In addition to these traditional EMT-related transcription factors, newly discovered transcription factors are also involved in the regulation of OS EMT. Among them is HOXC8, which is the focus of this study. In recent years, HOXC8 was found to promote EMT in triple-negative breast cancer by upregulating the transcription of MGP.[34] In addition, studies have also shown

that in non-small cell lung cancer, HOXC8 can inhibit the gene transcription of E-cadherin, thereby directly promoting the process of EMT.[35] In OS, HOXC8 has been reported to be involved in promoting tumor progression, but the specific mechanism has not been evaluated. In this study, we found that HOXC8 can act as a transcription factor to regulate the transcription of CDH2, and it binds to the 729–736 nucleotides of the CDH2 upstream promoter region. DLX2 can enhance the transcriptional effect of HOXC8 on CDH2 by binding to HOXC8. Our study revealed the role of HOXC8 in OS for the first time and showed that DLX2 could enhance the function of HOXC8. Meanwhile, it is worth noting that either targeting DLX2 or HOXC8 results in different effects on the expression of CDH2 and vimentin, which indicates that DLX2 is selective for the enhancement of HOXC8, and HOXC8 may have multiple regulatory mechanisms. Hence, it would be prudent to avoid generalizing the conclusions of this study to other EMT related. Further research into alternate regulatory mechanisms of HOXC8 is also warranted.

The results of our study are translatable to the clinic. Studies have shown that EMT may promote doxorubicin resistance.[36] In gastric cancer, resveratrol can inhibit EMT by regulating the PI3K/AKT signaling pathway, thereby reversing doxorubicin resistance.[37] The sensitivity of breast cancer to doxorubicin is also regulated by estrogen receptors to E-cadherin.[38] In this study, we revealed the link between DLX2 and doxorubicin resistance for the first time, and our results show that targeting DLX2 can significantly enhance the drug sensitivity of doxorubicin-resistant U-2OS cells and reduce CDH2 expression in drug-resistant cell lines. Our findings can provide new ideas for the treatment of patients with doxorubicin-resistant OS.

Limitation of the study

It is worth mentioning that our study has its limitations. Our findings show that DLX2 can only regulate the transcription of CDH2 through HOXC8 and is not able to regulate other EMT-related genes such as vimentin. In addition, other mechanisms of doxorubicin resistance remain unclear, and more investigation must be conducted before DLX2 targeting can be meaningfully translated to clinical practice. Still, our study highlights the potential value of targeting DLX2 in the treatment of OS, revealed a new mechanism of OS metastasis and doxorubicin resistance, and can direct novel treatment options for this debilitating disease and yet-unsolved problem.

STAR★METHODS

Detailed methods are provided in the online version of this paper and include the following:

- KEY RESOURCES TABLE
- RESOURCE AVAILABILITY
  - Lead contact
  - Materials availability
  - Data and code availability
- EXPERIMENTAL MODEL AND STUDY PARTICIPANT DETAILS
  - Ethical approval
  - Use of osteosarcoma patients' tissue
  - *In vivo* animal experiments
  - Cell culture
- METHOD DETAILS
  - Data collection
  - Cell culture and U2OS-DoxR formation
  - Immunohistochemistry (IHC)
  - RNA extraction, PCR and qPCR
  - Protein extraction and Western blot
  - Primers, antibodies, reagents and plasmids
  - Chromatin immunoprecipitation (ChIP) and Co-immunoprecipitation (Co-IP)
  - GST-pulldown
  - CCK-8
  - Colony formation
  - Transwell
  - *In vivo* experiment
- QUANTIFICATION AND STATISTICAL ANALYSIS

SUPPLEMENTAL INFORMATION

Supplemental information can be found online at https://doi.org/10.1016/j.isci.2023.108272.

ACKNOWLEDGMENTS

This work was supported by The Henan Science and Technology Research Project (grant number: 222102310004).

AUTHOR CONTRIBUTIONS

Conceptualization, B.Z., X.D., and W.Y.; Software, B.Z.; Investigation, B.Z. and X.D.; Resources, B.Z. and Y.F.; Writing – Original Draft, B.Z., X.D., and G.Q; Writing – Review & Editing, L.K.P and R.Z.; Formal analysis, X.D.; Visualization, B.Z. and Y.F; Supervision, B.Z., X.D., and W.Y.; Validation, X.D. and Y.F.; Funding acquisition, B.Z. and W.Y.; Project administration, B.Z. and W.Y.

DECLARATION OF INTERESTS

The authors declare no competing interests.

INCLUSION AND DIVERSITY

We support inclusive, diverse, and equitable conduct of research.

Received: June 12, 2023
Revised: September 13, 2023
Accepted: October 17, 2023
Published: October 19, 2023

REFERENCES

1. Siegel, R.L., Miller, K.D., Fuchs, H.E., and Jemal, A. (2021). Cancer Statistics, 2021. CA. Cancer J. Clin. *71*, 7–33. [published Online First: Epub Date]|. https://doi.org/10.3322/caac.21654.
2. Anderson, M.E. (2016). Update on Survival in Osteosarcoma. Orthop. Clin. North Am. *47*, 283–292. [published Online First: Epub Date]|. https://doi.org/10.1016/j.ocl.2015.08.022.
3. Simon, M.A. (1984). Causes of increased survival of patients with osteosarcoma: current controversies. J. Bone Joint Surg. Am. *66*, 306–310.
4. Nieto, M.A., Huang, R.Y.J., Jackson, R.A., and Thiery, J.P. (2016). Emt: 2016. Cell *166*, 21–45. https://doi.org/10.1016/j.cell.2016.06.028.
5. Brabletz, T. (2012). To differentiate or not–routes towards metastasis. Nat. Rev. Cancer *12*, 425–436. https://doi.org/10.1038/nrc3265.
6. De Craene, B., and Berx, G. (2013). Regulatory networks defining EMT during cancer initiation and progression. Nat. Rev. Cancer *13*, 97–110. https://doi.org/10.1038/nrc3447.
7. Zhou, Y., Zang, X., Huang, Z., and Zhang, C. (2013). TWIST interacts with endothelin-1/endothelin A receptor signaling in osteosarcoma cell survival against cisplatin. Oncol. Lett. *5*, 857–861. https://doi.org/10.3892/ol.2013.1111.
8. Shen, A., Zhang, Y., Yang, H., Xu, R., and Huang, G. (2012). Overexpression of ZEB1 relates to metastasis and invasion in osteosarcoma. J. Surg. Oncol. *105*, 830–834. https://doi.org/10.1002/jso.23012.
9. Yang, G., Yuan, J., and Li, K. (2013). EMT transcription factors: implication in osteosarcoma. Med. Oncol. *30*, 697. https://doi.org/10.1007/s12032-013-0697-2.
10. Wang, T., Wang, D., Zhang, L., Yang, P., Wang, J., Liu, Q., Yan, F., and Lin, F. (2019). The TGFbeta-miR-499a-SHKBP1 pathway induces resistance to EGFR inhibitors in osteosarcoma cancer stem cell-like cells. J. Exp. Clin. Cancer Res. *38*, 226. https://doi.org/10.1186/s13046-019-1195-y.
11. Sheng, G., Gao, Y., Yang, Y., and Wu, H. (2021). Osteosarcoma and Metastasis. Front. Oncol. *11*, 780264. https://doi.org/10.3389/fonc.2021.780264.
12. Lee, D.F., Su, J., Kim, H.S., Chang, B., Papatsenko, D., Zhao, R., Yuan, Y., Gingold, J., Xia, W., Darr, H., et al. (2015). Modeling familial cancer with induced pluripotent stem cells. Cell *161*, 240–254. https://doi.org/10.1016/j.cell.2015.02.045.
13. Lin, Y.H., Jewell, B.E., Gingold, J., Lu, L., Zhao, R., Wang, L.L., and Lee, D.F. (2017). Osteosarcoma: Molecular Pathogenesis and iPSC Modeling. Trends Mol. Med. *23*, 737–755. https://doi.org/10.1016/j.molmed.2017.06.004.
14. Tu, J., Huo, Z., Yu, Y., Zhu, D., Xu, A., Huang, M.F., Hu, R., Wang, R., Gingold, J.A., Chen, Y.H., et al. (2022). Hereditary retinoblastoma iPSC model reveals aberrant spliceosome function driving bone malignancies. Proc. Natl. Acad. Sci. USA *119*, e2117857119. https://doi.org/10.1073/pnas.2117857119.
15. Kim, H., Yoo, S., Zhou, R., Xu, A., Bernitz, J.M., Yuan, Y., Gomes, A.M., Daniel, M.G., Su, J., Demicco, E.G., et al. (2018). Oncogenic role of SFRP2 in p53-mutant osteosarcoma development via autocrine and paracrine mechanism. Proc. Natl. Acad. Sci. USA *115*, E11128–E11137. https://doi.org/10.1073/pnas.1814044115.
16. Jewell, B.E., Xu, A., Zhu, D., Huang, M.F., Lu, L., Liu, M., Underwood, E.L., Park, J.H., Fan, H., Gingold, J.A., et al. (2021). Patient-derived iPSCs link elevated mitochondrial respiratory complex I function to osteosarcoma in Rothmund-Thomson syndrome. PLoS Genet. *17*, e1009971. https://doi.org/10.1371/journal.pgen.1009971.
17. Tian, Z., Niu, X., and Yao, W. (2020). Receptor Tyrosine Kinases in Osteosarcoma Treatment: Which Is the Key Target? Front. Oncol. *10*, 1642. https://doi.org/10.3389/fonc.2020.01642.
18. Wang, X., Qin, G., Liang, X., Wang, W., Wang, Z., Liao, D., Zhong, L., Zhang, R., Zeng, Y.X., Wu, Y., and Kang, T. (2020). Targeting the CK1alpha/CBX4 axis for metastasis in osteosarcoma. Nat. Commun. *11*, 1141. https://doi.org/10.1038/s41467-020-14870-4.
19. Nomura, M., Rainusso, N., Lee, Y.C., Dawson, B., Coarfa, C., Han, R., Larson, J.L., Shuck, R., Kurenbekova, L., and Yustein, J.T. (2019). Tegavivint and the beta-Catenin/ALDH Axis in Chemotherapy-Resistant and Metastatic Osteosarcoma. J. Natl. Cancer Inst. *111*, 1216–1227. https://doi.org/10.1093/jnci/djz026.
20. Qiu, M., Bulfone, A., Ghattas, I., Meneses, J.J., Christensen, L., Sharpe, P.T., Presley, R., Pedersen, R.A., and Rubenstein, J.L. (1997). Role of the Dlx homeobox genes in proximodistal patterning of the branchial arches: mutations of Dlx-1, Dlx-2, and Dlx-1 and -2 alter morphogenesis of proximal skeletal and soft tissue structures derived from the first and second arches. Dev. Biol. *185*, 165–184. https://doi.org/10.1006/dbio.1997.8556.
21. Qiu, M., Bulfone, A., Martinez, S., Meneses, J.J., Shimamura, K., Pedersen, R.A., and Rubenstein, J.L. (1995). Null mutation of Dlx-2 results in abnormal morphogenesis of proximal first and second branchial arch derivatives and abnormal differentiation in the forebrain. Genes Dev. *9*, 2523–2538. https://doi.org/10.1101/gad.9.20.2523.
22. Anderson, S.A., Qiu, M., Bulfone, A., Eisenstat, D.D., Meneses, J., Pedersen, R., and Rubenstein, J.L. (1997). Mutations of the homeobox genes Dlx-1 and Dlx-2 disrupt the striatal subventricular zone and differentiation of late born striatal neurons. Neuron *19*, 27–37. https://doi.org/10.1016/s0896-6273(00)80345-1.
23. de Melo, J., Du, G., Fonseca, M., Gillespie, L.A., Turk, W.J., Rubenstein, J.L.R., and Eisenstat, D.D. (2005). Dlx1 and Dlx2 function is necessary for terminal differentiation and survival of late-born retinal ganglion cells in the developing mouse retina. Development *132*, 311–322. https://doi.org/10.1242/dev.01560.
24. Chiba, S., Takeshita, K., Imai, Y., Kumano, K., Kurokawa, M., Masuda, S., Shimizu, K., Nakamura, S., Ruddle, F.H., and Hirai, H. (2003). Homeoprotein DLX-1 interacts with Smad4 and blocks a signaling pathway from activin A in hematopoietic cells. Proc. Natl. Acad. Sci. USA *100*, 15577–15582. https://doi.org/10.1073/pnas.2536757100.
25. Tan, Y., Sementino, E., Pei, J., Kadariya, Y., Ito, T.K., and Testa, J.R. (2015). Co-targeting of Akt and Myc inhibits viability of lymphoma cells from Lck-Dlx5 mice. Cancer Biol. Ther. *16*, 580–588. https://doi.org/10.1080/15384047.2015.1018495.
26. Lee, S.Y., Jeon, H.M., Ju, M.K., Jeong, E.K., Kim, C.H., Yoo, M.A., Park, H.G., Han, S.I., and

Kang, H.S. (2015). Dlx-2 is implicated in TGF-beta- and Wnt-induced epithelial-mesenchymal, glycolytic switch, and mitochondrial repression by Snail activation. Int. J. Oncol. *46*, 1768–1780. https://doi.org/10.3892/ijo.2015.2874.

27. Yan, Z.H., Bao, Z.S., Yan, W., Liu, Y.W., Zhang, C.B., Wang, H.J., Feng, Y., Wang, Y.Z., Zhang, W., You, G., et al. (2013). Upregulation of DLX2 confers a poor prognosis in glioblastoma patients by inducing a proliferative phenotype. Curr. Mol. Med. *13*, 438–445.
28. Saitoh, M. (2018). Involvement of partial EMT in cancer progression. J. Biochem. *164*, 257–264. https://doi.org/10.1093/jb/mvy047.
29. Pastushenko, I., and Blanpain, C. (2019). EMT Transition States during Tumor Progression and Metastasis. Trends Cell Biol. *29*, 212–226. https://doi.org/10.1016/j.tcb.2018.12.001.
30. Wu, J., Liao, Q., He, H., Zhong, D., and Yin, K. (2014). TWIST interacts with beta-catenin signaling on osteosarcoma cell survival against cisplatin. Mol. Carcinog. *53*, 440–446. https://doi.org/10.1002/mc.21991.
31. Okamura, H., Yoshida, K., and Haneji, T. (2009). Negative regulation of TIMP1 is mediated by transcription factor TWIST1. Int. J. Oncol. *35*, 181–186. https://doi.org/10.3892/ijo_00000327.
32. Yang, H., Zhang, Y., Zhou, Z., Jiang, X., and Shen, A. (2011). Snail-1 regulates VDR signaling and inhibits 1,25(OH)-D(3) action in osteosarcoma. Eur. J. Pharmacol. *670*, 341–346. https://doi.org/10.1016/j.ejphar.2011.09.160.
33. Sharili, A.S., Allen, S., Smith, K., Hargreaves, J., Price, J., and McGonnell, I. (2011). Expression of Snail2 in long bone osteosarcomas correlates with tumour malignancy. Tumour Biol. *32*, 515–526. https://doi.org/10.1007/s13277-010-0146-1.
34. Gong, C., Zou, J., Zhang, M., Zhang, J., Xu, S., Zhu, S., Yang, M., Li, D., Wang, Y., Shi, J., and Li, Y. (2019). Upregulation of MGP by HOXC8 promotes the proliferation, migration, and EMT processes of triple-negative breast cancer. Mol. Carcinog. *58*, 1863–1875. https://doi.org/10.1002/mc.23079.
35. Zhang, J., Yang, M., Li, D., Zhu, S., Zou, J., Xu, S., Wang, Y., Shi, J., and Li, Y. (2019). Homeobox C8 is a transcriptional repressor of E-cadherin gene expression in non-small cell lung cancer. Int. J. Biochem. Cell Biol. *114*, 105557. https://doi.org/10.1016/j.biocel.2019.06.005.
36. Mirzaei, S., Abadi, A.J., Gholami, M.H., Hashemi, F., Zabolian, A., Hushmandi, K., Zarrabi, A., Entezari, M., Aref, A.R., Khan, H., et al. (2021). The involvement of epithelial-to-mesenchymal transition in doxorubicin resistance: Possible molecular targets. Eur. J. Pharmacol. *908*, 174344. https://doi.org/10.1016/j.ejphar.2021.174344.
37. Xu, J., Liu, D., Niu, H., Zhu, G., Xu, Y., Ye, D., Li, J., and Zhang, Q. (2017). Resveratrol reverses Doxorubicin resistance by inhibiting epithelial-mesenchymal transition (EMT) through modulating PTEN/Akt signaling pathway in gastric cancer. J. Exp. Clin. Cancer Res. *36*, 19. https://doi.org/10.1186/s13046-016-0487-8.
38. Wan, X., Hou, J., Liu, S., Zhang, Y., Li, W., Zhang, Y., and Ding, Y. (2021). Estrogen Receptor alpha Mediates Doxorubicin Sensitivity in Breast Cancer Cells by Regulating E-Cadherin. Front. Cell Dev. Biol. *9*, 583572. https://doi.org/10.3389/fcell.2021.583572.

STAR★METHODS

KEY RESOURCES TABLE

REAGENT or RESOURCE	SOURCE	IDENTIFIER
Antibodies		
DLX2 Polyclonal antibody	Proteintech (Wuhan Sanying, Wuhan, China)	Cat#26244-1-AP
DLX2 Immunoprecipitation Antibody	Invitrogen (ThermoFisher Scientific, Shanghai, China)	Cat#702009
Beta Actin Monoclonal antibody	Proteintech (Wuhan Sanying, Wuhan, China)	Cat#66009-1-Ig
Anti-E Cadherin antibody [HECD-1]	Abcam (Shanghai, China)	Cat#ab40772
Anti-N Cadherin antibody	Abcam (Shanghai, China)	Cat#ab18203
Vimentin Polyclonal antibody	Proteintech (Wuhan Sanying, Wuhan, China)	Cat#10336-1-AP
TWIST1-specific Polyclonal antibody	Proteintech (Wuhan Sanying, Wuhan, China)	Cat#25465-1-AP
Anti-MMP2 antibody	Abcam (Shanghai, China)	Cat#ab97779
HOXC8 Polyclonal antibody	Proteintech (Wuhan Sanying, Wuhan, China)	Cat#15448-1-AP
HOXC8 immunoprecipitation antibody	Santa Cruz Biotechnology	Cat#sc-517007
Rabbit IgG control Polyclonal antibody	Proteintech (Wuhan Sanying, Wuhan, China)	Cat#30000-0-AP
GST Tag Polyclonal antibody	Proteintech (Wuhan Sanying, Wuhan, China)	Cat#10000-0-AP
Goat Anti-Rabbit IgG H&L (HRP)	Abcam (Shanghai, China)	Cat#ab6721
Goat Anti-Mouse IgG H&L (HRP)	Abcam (Shanghai, China)	Cat#ab6789
Bacterial and virus strains		
DLX2 shRNA (lentivirus)	GeneChem Co., Ltd (Shanghai, China)	5′-CTGAAATTCGGATAGTGAA-3′
HOXC8 shRNA (lentivirus)	GeneChem Co., Ltd (Shanghai, China)	5′-UGGGACUGACCGAGAGACAAGUGAA-3′
BL21 Escherichia coli	Solarbio (Beijing, China)	Cat#C1400
Biological samples		
BALB/cA-nu Mice (SPF grade)	Beijing HFK Bioscience Co., LTD (Beijing, China)	BALB/cA-nu Mice
Critical commercial assays		
Trizol	Invitrogen (ThermoFisher Scientific, Shanghai, China)	Cat#15596026
RevertAid First Strand cDNA Synthesis Kit	ThermoFisher (ThermoFisher Scientific, Shanghai, China)	Cat#K1621
FastStart Universal SYBR Green Master Mix (ROX)	Roche (Shanghai, China)	Cat#4913850001
SDS-PAGE gel preparation kit	Solarbio (Beijing, China)	Cat#P1200
SDS-PAGE loading buffer, 5X (with DTT)	Solarbio (Beijing, China)	Cat#P1040
PageRuler pre-stained protein ladder	ThermoFisher (Shanghai, China)	Cat#26616
Pierce Classic Magenetic IP/Co-IP Kit	ThermoFisher (Shanghai, China)	Cat#88804
Pierce GST protein interaction Pull-Down Kit	ThermoFisher (Shanghai, China)	Cat#21516
Pierce Renilla-Firefly Luciferase Dual Assay Kit	ThermoFisher (Shanghai, China)	Cat#16185
10000X SolarRed nucleic acid dyes	Solarbio (Beijing, China)	Cat#G5560
Doxorubicin	MedChemExpress (Shanghai, China)	Cat#HY-15142A
CCK-8 kit	Dojindo China (Beijing, China)	Cat#CK04

(*Continued on next page*)

Continued

REAGENT or RESOURCE	SOURCE	IDENTIFIER
Deposited data		
TARGET Osteosarcoma RNA-Seq	TARGET Database(https://www.cancer.gov/ccg/research/genome-sequencing/target); GDC portal of TCGA (https://gdc.cancer.gov/access-data/gdc-data-portal)	TARGET Database(https://www.cancer.gov/ccg/research/genome-sequencing/target) and GDC(https://gdc.cancer.gov/access-data/gdc-data-portal)
GSE87624	GEO website (https://www.ncbi.nlm.nih.gov/geo/query/acc.cgi?acc=GSE87624)	GEO website (https://www.ncbi.nlm.nih.gov/geo/query/acc.cgi?acc=GSE87624)
Experimental models: Cell lines		
hFOB-1.19	the Cell Bank of the Chinese Academy of Sciences	hFOB-1.19
MG-63	the Cell Bank of the Chinese Academy of Sciences	MG-63
U2OS	the Cell Bank of the Chinese Academy of Sciences	U2OS
143B	American Type Culture Collection	143B[CRL-8303]
Experimental models: Organisms/strains		
BALB/cA-nu Mice (SPF grade)	Beijing HFK Bioscience Co., LTD (Beijing, China)	BALB/cA-nu Mice
Oligonucleotides		
	See Table S1	
Recombinant DNA		
CDH2 mutation plasmids	Sangon Biotech Co., Ltd	Sangon Biotech
DLX2 GST plasmids	Sangon Biotech Co., Ltd	Sangon Biotech
HOXC8 GST plasmids	Sangon Biotech Co., Ltd	Sangon Biotech
Software and algorithms		
R Ver. 4.0.3	the R Project for Statistical Computing	R cran
GraphPad Prism 9	GraphPad	GraphPad Prism 9

RESOURCE AVAILABILITY

Lead contact

Further information and requests for resources and reagents should be directed to and will be fulfilled by the lead contact, Boya Zhang (zlyyzhangboya@163.com).

Materials availability

qPCR primers of DLX2, HOXC8, CDH1, CDH2, VIM (Vimentin), TWIST1, MMP2, GAPDH and PCR-729 primers used in HOXC8 ChIP experiment are generated by Sangon Biotech (Shanghai) Co., Ltd (Shanghai, China). Lentivirus targeting DLX2 or HOXC8, HOXC8 overexpression plasmids, CDH2 mutation plasmids and plasmids used in GST pulldown experiments are generated by Sangon Biotech Co., Ltd (Shanghai, China). Doxorubicin resistant U2OS cell line (U2OS-DoxR) was generated by the author Boya Zhang.

Data and code availability

- This paper analyzes existing, publicly available data. Osteosarcoma sequencing data of TARGET database was downloaded from the "Therapeutically Applicable Research To Generate Effective Treatments" (*URL:* https://ocg.cancer.gov/programs/target)and "National Cancer Institute GDC Data Portal" Website (*URL:* https://gdc.cancer.gov/access-data/gdc-data-portal). Data of GSE87624 was downloaded from GEO website (*URL:* https://www.ncbi.nlm.nih.gov/geo/query/acc.cgi?acc=GSE87624). Related accession numbers are listed in the key resources table.
- This paper does not report original code.
- Any additional information required to reanalyze the data reported in this paper is available from the lead contact upon request.

EXPERIMENTAL MODEL AND STUDY PARTICIPANT DETAILS

Ethical approval

This experiment was approved by the Ethics Committee of Henan Cancer Hospital (Ethics approval number: 2022-KY-0055-001). All procedure has acquired patients or their guardians' written consent permission.

Use of osteosarcoma patients' tissue

The selected participants are adolescents under the age of 18, with no gender restrictions. All patients have a psychological gender identity consistent with their biological gender and belong to the Han Chinese ethnic group. Their educational levels are in line with the average for their respective age groups. This study collected samples from 12 individuals, and relevant information can be found in Table 1. All samples are biopsy specimens. All patients or their guardians were informed of this and consented to the use of their tumor samples in this study.

In vivo animal experiments

In these experiments, female BALB/cA-nu nude mice at five weeks of age were used, with an average weight of 20 g and a weight range of ±5 g. These mice lack thymus, rendering them immunodeficient. Furthermore, this batch of nude mice had not been previously exposed to any drugs or subjected to any experiments. They were housed at the Henan Provincial Experimental Animal Center under specific pathogen-free (SPF) conditions, featuring dedicated barrier systems and independent air supply. Five nude mice were co-housed in each cage, provided with standard rodent chow, and maintained at a controlled room temperature ranging from 20°C to 26°C. Cage bedding was changed every three days to ensure proper hygiene. Regarding the experimental grouping, all mice were gathered together, and group allocation was performed by random selection, resulting in equal-sized groups.

Cell culture

In this study, four mature cell lines were utilized, namely hFOB-1.19, MG-63, U2OS, and 143B. The hFOB-1.19, MG-63, and U2OS cell lines were sourced from the Cell Bank of the Chinese Academy of Sciences (https://www.cellbank.org.cn), while the 143B cell line was obtained from the American Type Culture Collection (https://www.atcc.org). MG-63, U2OS, and 143B cells were cultured in a cell culture incubator with a 5% carbon dioxide concentration and a constant temperature of 37°C. The complete culture medium used was high-glucose DMEM supplemented with 10% fetal bovine serum, and an appropriate concentration of penicillin-streptomycin was added to prevent potential contamination. hFOB-1.19 cells were cultured in DMEM/F12 (1:1) (1X) medium (GIBCO, Cat.11320033) with the addition of G418 at a concentration of 0.3 mg/mL (Solarbio Life Science, Cat.G8161). The fetal bovine serum concentration was 10%, and the culture temperature was maintained at 33.5°C. The incubator for hFOB-1.19 cells also contained 5% carbon dioxide.

METHOD DETAILS

Data collection

Data from the TARGET database were obtained through The Therapeutically Applicable Research to Generate Effective Treatments website (https://ocg.cancer.gov/programs/target), specifically at data level 3. The GSE87624 dataset was retrieved from the SRA database (https://www.ncbi.nlm.nih.gov/sra) using the sratoolkit for downloading.

Regarding clinical samples, all patient specimens were procured during surgical procedures or needle biopsies. These samples were promptly preserved in either formalin or RNA protective solution and stored in strict adherence to the prescribed guidelines. Clinical data have been systematically organized based on the results of follow-up assessments conducted at three-month intervals.

Cell culture and U2OS-DoxR formation

U-2OS, MG63, 143B, and hFOB-1.19 cell lines were procured from ATCC and maintained at 37°C in a cell incubator with 5% CO2. The culture medium employed was DMEM supplemented with 10% fetal bovine serum. Additionally, the antibiotic included in the medium was Primocin (Invitrogen, USA), specifically, 1 mL of Primocin was added per 500 mL of complete medium.

U2OS-DoxR cells were generated using the following method: Initially, normally proliferating U2OS cells were selected, passaged for 24 h, and allowed to adhere to the culture dish. Subsequently, 0.015 μg/mL of doxorubicin was added, and the medium was changed daily until the cells resumed normal growth after passaging. The doxorubicin concentration was gradually increased to 0.02 μg/mL. This process was iterated with increasing concentrations of 0.03 μg/mL, 0.05 μg/mL, 0.07 μg/mL, 0.09 μg/mL, 0.1 μg/mL, 0.12 μg/mL, 0.14 μg/mL, 0.16 μg/mL, 0.18 μg/mL, 0.2 μg/mL, 0.3 μg/mL, and 0.5 μg/mL, until the cells could proliferate normally in the presence of 0.5 μg/mL doxorubicin. Successful establishment of the U2OS-DoxR cell line was confirmed. Subsequently, the cells were cultured in DMEM containing 0.5 μg/mL doxorubicin and 10% fetal bovine serum.

Immunohistochemistry (IHC)

The dewaxed paraffin sections were subjected to incubation for 5–10 min at room temperature with a 3% H2O2 solution to eliminate endogenous peroxidase activity. Afterward, they were rinsed with distilled water and immersed in PBS for 5 min, repeated twice. Antigen retrieval was performed using sodium citrate, with high heat for 5 min, followed by medium-low heat for 7 min. Subsequently, the sections were

blocked with 5–10% normal goat serum (diluted in PBS). The blocking step occurred at room temperature for 10 min, the serum was then poured off without washing. The primary antibody was added dropwise and incubated either at 37°C for 1–2 h or overnight at 4°C. After the primary antibody incubation, the sections were rinsed with PBS, 5 min each for a total of 3 washes. Next, an appropriate amount of biotin-labeled secondary antibody working solution was added dropwise and incubated at 37°C for 10–30 min. Following this incubation, the sections were again rinsed with PBS, 5 min each for 3 washes. An appropriate amount of horseradishase or alkaline phosphatase-labeled streptavidin working solution was then added dropwise and incubated at 37°C for 10–30 min. The sections were subsequently rinsed with PBS, 5 min each for 3 washes. The color reagent was allowed to develop for 3–15 min (using DAB), followed by a rinse with tap water. Afterward, the sections were counterstained, dehydrated, made transparent, and mounted.

RNA extraction, PCR and qPCR

Wash the cells with PBS, centrifuge the cells, discard the supernatant, add 1 mL of Trizol reagent, mix thoroughly, add 200 μl chloroform, invert and mix well, let stand at 4°C for 15 min, and then centrifuge at 4°C and 12,000 rpm for 15 min. After centrifugation, take 500ul of supernatant, add the same amount of isopropanol and mix upside down, let stand at 4°C for 10 min, then centrifuge at 4°C and 12000 rpm for 10 min, discard the supernatant, add 1 mL of 75% Water ethanol, invert upside down and mix, centrifuge at 4°C and 7500 rpm for 5 min. Discard the supernatant, place it upside down on absorbent paper, and place it in a fume hood to dry for 5 min. Then 20 μL of enzyme-free water was added to the pellet, and the RNA concentration was measured in time.

cDNA reverse transcription was performed using the RevertAid First Strand cDNA Synthesis Kit (Thermo, USA) and in strict accordance with the instructions. The amount of RNA used in a single reaction system was 5ug.

The reaction system of qPCR is as follows: 1). FastStart Universal SYBR Green Master (Rox), 10 μL; 2). cDNA, 2μL; 3). Forward primer, 1μL; 4). Reverse primer, 1μL; 5). Enzyme-free water, 6μL.

Protein extraction and Western blot

Extraction of cellular and tissue proteins was done using RIPA. For the cells, the medium was discarded and washed with PBS, then an appropriate amount of RIPA was added, placed at 4°C for 30 min, and centrifuged at 12,000 rpm for 30 min at 4°C. Subsequently, the supernatant was aspirated, the protein concentration was determined by Bradford method, and stored at −80°C for later use.

For Western blot, mix protein and 5X loading buffer 4:1 and heat at 95°C for 5 min. The samples were then added to a 10% SDS-PAGE gel for electrophoresis. Electroporation was carried out with PVDF membrane, 250 mA constant current for 120 min, then blocked with 5% nonfat milk powder for 1 h, washed three times with TBST, and incubated with the corresponding primary antibody overnight at 4°C. The next day, the primary antibody was taken out, washed three times with TBST, then incubated with the corresponding secondary antibody for 1 h, washed three times with TBST, and then photographed.

Primers, antibodies, reagents and plasmids

Details in Table S1. It should be specially pointed out that the lentivirus, GST pull-down plasmids and CDH2 promoter mutation plasmid were all synthesized by Sangon Biotech Co., Ltd

Chromatin immunoprecipitation (ChIP) and Co-immunoprecipitation (Co-IP)

ChIP and Co-IP experiments were carried out according to the corresponding instructions (Table S1), and detected by PCR or Western blot.

GST-pulldown

GST pull-down were performed using the Pierce GST Protein Interaction Pull-Down Kit (Thermo scientific, USA), DLX2-GST and HOXC8-GST plasmids were conduct by Sangon Biotech Co., Ltd. As for fusion protein generation, Plasmids were transfected into BL21 Escherichia coli strains. All steps in GST pull-down are performed according to the corresponding instructions (Table S1). In short, 6 steps are needed: 1). bait protein preparation. 2). Bait protein immobilization. 3). Prey protein preparation. 4). prey protein capture. 5). Bait-prey elution. 6)gel analysis.

CCK-8

CCK-8 starts by seeding 1000 cells per well into a 96-well microplate at a predetermined density. Incubate the cells in a cell culture incubator at 37°C with 5% CO2 until they adhere to the plate surface and reach the desired experimental conditions. Carefully remove the cell culture medium from the wells without disturbing the cells. Add an appropriate volume of the CCK-8 working solution to each well, ensuring that all cells are covered. Return the plate to the cell culture incubator and allow it to incubate for a specific period, typically 2 h. After the incubation period, remove the plate from the incubator. Using a microplate reader, measure the absorbance of each well at 450 nm wavelength to determine the optical density (OD).

Colony formation

1000 transfected tumor cells were plated in a six-well plate. Add an appropriate amount of complete medium. After 7–10 days of culture, cells in the lower chamber were fixed with 4% paraformaldehyde, then stained with 1% crystal violet for 30 min at room temperature, and photographed for counting.

Transwell

8 μm Transwell chambers were selected, and 8000 OS tumor cells (U2OS, 143B) were inoculated in the upper chamber, and serum-free medium was added. Complete medium was added to the lower chamber, and after culturing in a cell incubator for 36 h, the chamber was fixed with 4% paraformaldehyde, then stained with 1% crystal violet at room temperature for 30 min, and the cells in the upper layer of the chamber were wiped off. Count 5 fields of view under the 20X objective lens.

In vivo experiment

We used 5-week-old nude mice for subcutaneous tumor implantation, with each mouse receiving 1x10^7 143B cells. Typically, one week later, the tumor diameter was approximately 2 mm. At this point, we injected adeno-associated viruses targeting DLX2 or serving as a negative control every other day and measured tumor size. After three weeks, all experimental subjects were euthanized, and the tumors were harvested for subsequent experiments.

The construction of the subcutaneous xenograft model to investigate doxorubicin sensitivity was carried out as follows: We used 5-week-old nude mice, with each mouse receiving 1x10^7 143B cells. Under normal conditions, approximately one week later, when the tumor diameter was about 2 mm, we administered either DLX2-targeting adenovirus or an adenovirus as a negative control. Tumor size was measured every other day. Starting on the 13th day (2 weeks), we initiated docetaxel treatment at a dosage of 4 mg/kg once a week. After one month of experimentation, all experimental subjects were euthanized, and the tumors were harvested for subsequent experiments.

The construction of the lung metastasis model to investigate the sensitivity to doxorubicin was as follows: We used 5-week-old nude mice and performed intravenous injections via the tail vein. Each mouse received either 5x10^6 143B cells or 143B cells with DLX2 knocked down. To mimic clinical conditions more accurately, we initiated doxorubicin treatment on the second day, administering it once a week at a dose of 4 mg/kg. After 4 weeks, all experimental subjects were euthanized, and lung tissues were harvested for subsequent experiments.

QUANTIFICATION AND STATISTICAL ANALYSIS

The statistical analysis software used in this study includes R (Version 4.0.3) and GraphPad Prism 9. the official software was used for GSEA. The primary R packages used are edgeR, ggplot2, Survminer, WGCNA and ggsci.

Differences in continuous variables between two groups were analyzed using the t-test, while differences in continuous variables among multiple groups were analyzed using ANOVA. Chi-square tests were used to analyze differences in categorical variables. The significance of differential gene expression was calculated using a Poisson distribution (default algorithm in the edgeR package). Error bars shown in the figures represent the mean $\pm$ SEM. In p value annotations, * represents $p < 0.05$, ** represents $p < 0.01$, *** represents $p < 0.001$, and **** represents $p < 0.0001$.

All R code used adheres to the instructions provided in the documentation of the respective R packages. The code was executed after changing variable names and debugging. If you have any questions, you can contact this e-mail address: zlyyzhangboya@163.com.